Conformation Dependence of pK_a: Ab Initio and DFT Investigation of Histidine

Péter Hudáky[†,‡] and András Perczel*[,†]

Department of Organic Chemistry and Department of Theoretical Chemistry, Eötvös L. University, H-1518 Budapest 112, P.O. Box 32, Hungary

Received: March 8, 2004; In Final Form: May 13, 2004

Proton affinity and pK_a values of *N*-formyl-L-histidinamide are found to vary as a function of its backbone and/or side-chain orientation. Proton affinities between the cationic and neutral forms of structurally similar conformers are between −246 and −230 kcal mol^{-1}, while pK_a values associated with the same conformers are between 6 and 8. For the neutral-to-anion transition, the following ranges were computed $-342 > PA > -350$ kcal mol^{-1} and $18 < pK_a < 22$. The protonation state of histidines on the surface of a protein depends primarily on the pH. Due to protonation or deprotonation, the side-chain and/or backbone orientation of these histidine residues may undergo considerable changes. Examples are presented and confirmed by ab initio calculations, where proteins were crystallized under various pH conditions, resulting in the same histidine residue to adopt different conformations. Furthermore, a hypothesis is given for a protonation-induced conformational modification of the histidine residue in the catalytic triad of chymotrypsin during catalysis, which lowers the pK_a value of the catalytic histidine by 1.2 units. Both the experimental and theoretical results support that proton affinity as well as that pK_a values of histidine residues are strongly conformationally dependent.

Introduction

In peptides and proteins, the conformation of a histidine residue is described with ω_o, φ, ψ, χ_1, and χ_2 torsion angles (Scheme 1). The first three of these five variables (ω_o, φ, ψ) determine the backbone, while χ_1 and χ_2 define the side-chain orientation of this amino acid residue. It has been shown that for most torsional angles of amino acid residues, the potential energy curve may have at most three minima.[1,2] As a consequence, the potential energy hypersurface (PEHS) of an amino acid diamide, may have a maximum of 3^n minima, where n is the number of dimensions of the appropriate PEHS. Thus, for histidine residue, where $n = 4$ (φ, ψ, χ_1, χ_2), a total of 81 different conformers are expected. In this study, only conformers with a trans amide bond ($\omega_o \approx 180°$) are considered. All minima of all four different states of protonation of *N*-formyl-L-histidinamide (Scheme 1) were recently determined[3,4] by ab initio computations, based on the $3^4 \times 4 = 324$ minima predicted by multidimensional conformation analysis (MDCA).[1] The number of minima found for *N*- and *C*-protected amino acid residues is found to be always less than the above-mentioned maximum number (3^n), regardless of the type of amino acid residue or the level of theory applied.[5−27] In the case of *N*-formyl-L-histidinamide, 129 out of the 324 structures were identified as minima[3,4] at the RHF/6-31G(d) level of theory. Conformational building units of well-known secondary structural elements, such as the right-handed α-helix (α_L) and that of polyproline II (ϵ_L), are usually not minima of either *N*-For-L-Xxx-NH_2 or *N*-Ac-L-Xxx-NHMe model systems.[5−27] However, for *N*-For-L-His-NH_2, theoretical calculations provided examples for both types of minima, due to favorable intraresidual interactions.[3,4]

The side chain of histidine has four different states of protonation as a function of its molecular environment, providing a perfect example of an amino acid residue with a multivariant nature. At different protonation states, the aromatic imidazole ring of histidine can be either a cation, a neutral aromatic residue, or even an anion. When neither nitrogen atom of the imidazole ring carries a proton, the side chain of histidine becomes negatively charged, denoted as His[−1] throughout this paper. A single proton can be attached in two alternative ways to the nitrogen atoms of His, namely, either at the π or at the τ position.[28] To refer these two forms, in this paper we use the notation His[N^{π}H] and His[N^{τ}H], respectively. (Note that N^{π} and N^{τ} are also referred to as N^{δ} and N^{ϵ}, respectively.) In both tautomeric forms the side chain is neutral and serves as a model for aromatic and polar but uncharged amino acid residues. Finally, if both nitrogen atoms of the imidazole carry a proton, the side chain of histidine is positively charged and denoted as His[+1] (Scheme 1).

Histidine can be modeled by imidazole[29] or alkyl-imidazole in theoretical calculations. The protonation states of 5-methylimidazole were studied previously.[30,31] The average total energy difference between the neutral and protonated forms was found to be 0.2887 Hartree (181.16 kcal mol^{-1}) at the DZP SCF level of theory.[30] The PA of 5-methylimidazole was predicted[31] to be 228.2 kcal mol^{-1}, while that of unprotected histidine amino acid is equal to 232.7 kcal mol^{-1}. However, these models do not have multiple different conformers, thus are unsuitable to determine the conformational dependence of both proton affinity (PA) and pK_a. The energy of protonation or deprotonation of unprotected amino acid residues was discussed,[32] but conformational dependence of PA and pK_a was not covered.

* Corresponding author. E-mail: perczel@para.chem.elte.hu. URL http://www.szerves.chem.elte.hu. Telephone (36-1)-209-0555 ext. 1653. Fax (36-1)-372-26-20.

† Department of Organic Chemistry.

‡ Department of Theoretical Chemistry.

10.1021/jp048964q CCC: $27.50
Published on Web 06/25/2004

SCHEME 1: Four Different Protonation Forms of *N*-Formyl-L-histidinamide: Indexation of Carbon and Nitrogen Atoms Is Shown on the Top, Location of Torsional Angles Is Shown on the Bottom Molecule

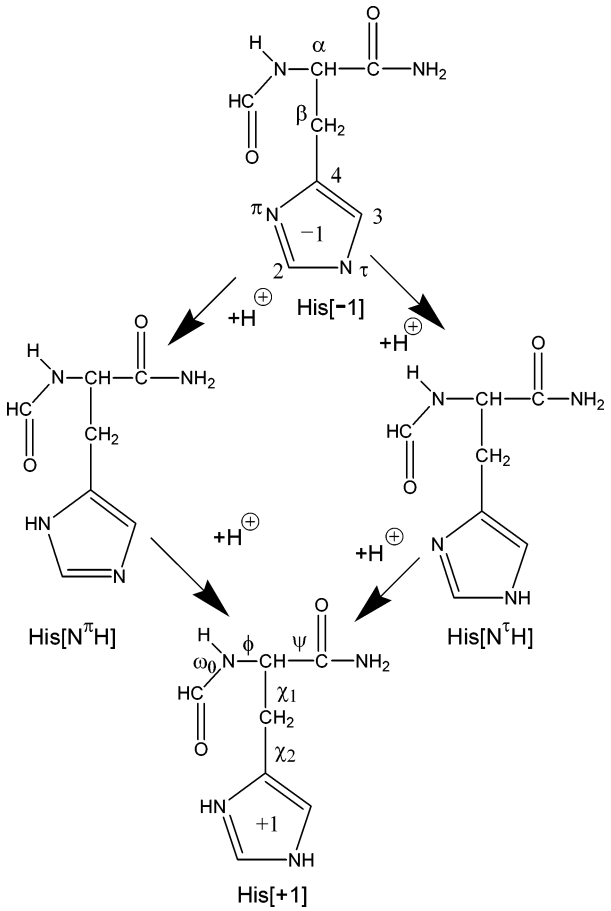

Note that N^{π}, N^{τ}, C^2, C^3, and C^4 are also referred to as N^{δ}, N^{ϵ}, C^{δ}, C^{ϵ} and C^{γ}, respectively.

The proton-transfer capability of the imidazole ring through its two side chain nitrogen atoms provides a key role for histidine to participate in different biological processes. Histidine takes an active role in the catalytic mechanism of serine proteases, being the proton-transfer medium between the aspartate and serine residues.[33,34] The conformational changes of histidine serve as an important mechanistic feature to create taxonomic substates in carbonmonoxy myoglobin.[35] Furthermore, histidine plays an important role in plasminogen activator inhibitor (PAI-1),[36] type I signal peptidases (SPases),[37] cysteine proteinases,[38] amylase,[39] hemophores (HasA),[40] and in many other enzymes. In numerous enzymatic reactions[41] the proton-transfer role of the imidazole ring requires conformational flexibility coupled with considerable dipole changes of histidine. Occasionally, structures are even stabilized through a $C^2-H\cdot\cdot O{=}C$ type (Scheme 1) of hydrogen bond.[33,42] Ab initio or DFT investigations of conformational and/or catalytic processes of enzymes recently became feasible.[43−46]

We carried out a detailed investigation on the reliability of theoretical pK_a calculations on small molecules with known pK_a and on histidine residues in proteins, where both conformation and pK_a could be experimentally determined. The correlation of calculated and experimental pK_a values is very significant in both cases. The present paper emphasizes the conformation-dependent nature of PA and pK_a and offers explanation for properties of histidine to clarify more of its versatile biological role.

SCHEME 2: Diagram of Steps for Calculation of the pK_a Value

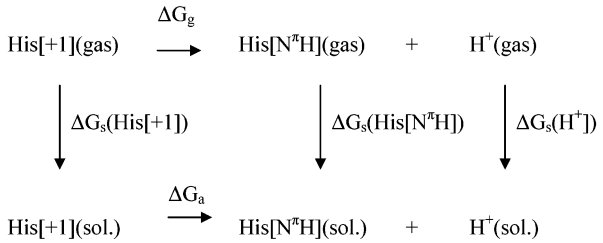

Methods

Computational Details. All computations associated with *N*-formyl-L-histidinamide were carried out by the GAUSSIAN 98 program package,[47] using the restricted Hartree−Fock theory (RHF)[48,49] and the standard 6-31G(d) basis set.[50−52] Geometries were optimized at the RHF/6-31G(d) level of theory[3,4] using the GDIIS optimization method. Additional constrained optimizations, as well as PA and pK_a calculations were now carried out for all conformers of *N*-formyl-L-histidinamide at the same level of theory. Constrained conformers mimicking the catalytic histidine in chymotrypsin were studied at RHF/6-311++G(d,p) and surface histidines of hemaphores at RB3LYP/6-311++G-(2d,2p) level of theory.

Proton affinity was determined for the anionic and neutral forms of *N*-formyl-L-histidinamide using eq 1:[53]

$$\mathrm{PA} = -\Delta H_r(298) = \Delta E_e(0) + \Delta E_v(0) + \Delta(\Delta E_v(298)) + 5/2RT \quad (1)$$

where PA is the proton affinity, $\Delta E_e(0)$ is the total electronic energy, $\Delta E_v(0)$ is the zero point vibration energy, $\Delta(\Delta E_v(298))$ is the change of vibration energy during heating from 0 to 298 K and $5/2RT$ is the classical term estimating the effect of losing three translational degrees of freedom. Values of pK_a were calculated[54−60] according to the thermodynamic cycle[61] presented for one of the neutral tautomers of histidine on Scheme 2.

The applied equation, as may be derived from the thermodynamic cycle, is stated in eq 2:

$$\mathrm{p}K_a = \frac{1}{2303RT}\Delta G_a = \frac{1}{2303RT}\{\Delta G_g + \Delta G_s(\mathrm{His}[N^{\pi}H]) - \Delta G_s(\mathrm{His}[+1]) + \Delta G_s(H^+)\} \quad (2)$$

where ΔG_g is the gas-phase free energy change for the deprotonation process and ΔG_s is the solvation free energy of the corresponding molecule or ion. The solvation free energy was calculated using the PCM[62] solvent model, with dielectric constant 78.39, appropriate for water. The solvation free energy of a proton is considered to be −263.86 kcal mol^{-1}.[63] Calculated pK_a values are scaled throughout the article using the linear regression parameters $m = 0.71$ and $b = 2.56$ for the values computed at RHF/6-31G(d) level of theory (determination of regression parameters is described in the results).

Protein Data Base Analysis. All investigated protein structures were taken from the 2003 version of the PDB.[64] All entries correspond to high-resolution X-ray structures.

Nomenclature for Backbone and Side-Chain Conformers. The $E = E(\varphi,\psi)$ PES, also called Ramachandran map,[65] can be subdivided into catchment regions or conformational subregions in alternative ways. For the pair of torsional angles (φ and ψ) used to describe the backbone fold of peptides and

SCHEME 3: (A) Ideal Location of the Nine Typical Backbone Folds of Peptides on the $E = E(\varphi,\psi)$ Surface Labeled According to the IUPAC−IUB Guidance

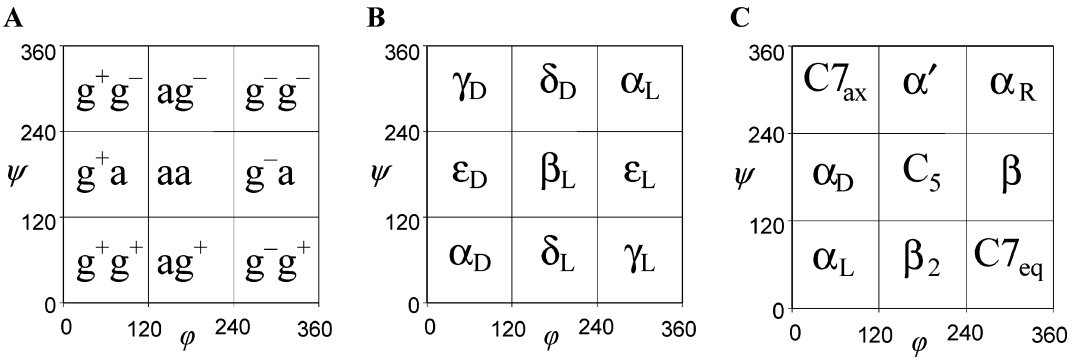

Torsion angle coordinates are drawn from 0° to 360°. The ideal location of the nine typical backbone folds of peptides. **(B)** Applied short-hand notation of all nine minima. **(C)** An alternative labeling applied in several crystallographic papers.

proteins, multidimensional conformational analysis (MDCA) predicts nine clearly defined subregions, as depicted in Scheme 3. Following the recommendation of IUPAC−IUB the gauche+ (g+), anti (a), and gauche− (g−) descriptors could be used for labeling different conformers. However, we save gauche+, anti, and gauche− to describe side chain rotamers (see below). Thus the following scheme has been introduced to describe the nine alternative backbone structures: $\alpha_L \equiv$ (g−g−), $\alpha_D \equiv$ (g+g+), $\beta_L \equiv$ (aa), $\gamma_L \equiv$ (g−g+), $\gamma_D \equiv$ (g+g−), $\delta_L \equiv$ (ag+), $\delta_D \equiv$ (ag−), $\epsilon_L \equiv$ (g−a), and $\epsilon_D \equiv$ (g+a) (Scheme 3).

In *N*-formyl-L-histidinamide, which contains two geminal H^β and an imidazole ring attached to C^β, distinct χ_1 and χ_2 rotamers are expected. Thus, the three predicted orientations gauche+, anti, and gauche− (+, a, − in short) about both χ_1 and χ_2 will differ energetically. The conventional definition of χ_1 ($N-C^\alpha-C^\beta-C^4$) and that of χ_2 ($C^\alpha-C^\beta-C^4-N^\pi$) was used (Scheme 1).

Conformational Shift during Proton Transfer. A proton transfer is usually coupled with a conformational change. This is taken into account in pK_a calculations by using the appropriate conformers that may be distinct in each protonation state. In this way minimum energy structures are considered both in protonated and deprotonated forms. However, in some cases, we define theoretical pK_a calculations on "frozen" conformers, where flexible torsional angles are fixed. During this procedure all calculations are carried out with torsional angles forced to take a specific value, ensuring the result to correspond to the desired conformation. In this case, according to the investigated case, conformation of protonated and deprotonated forms may be the same or may differ.

Results

Precision and Accuracy. Selection of the level of theory determines both precision of the calculation and the size of the molecular system to be investigated. The middle sized RHF/6-31G(d) level of theory was chosen due to its applicability for larger biomolecules. Comparing experimental and calculated pK_a values (Figure 1) for nitrogen-containing heterocyclic molecules, an almost perfect agreement was observed ($R^2_{calc.\leftrightarrow exp.} = 0.995$). Similarly, using a significantly larger basis set and a method involving electron correlation (RB3LYP/6-311++G(2d,2p)), the correlation coefficient is also high ($R^2_{calc.\leftrightarrow exp.} = 0.973$). Using the appropriate regression parameters (e.g., $m = 0.71$ and $b = 2.56$), computed pK_a values match experimental counterparts within ±0.5 unit.

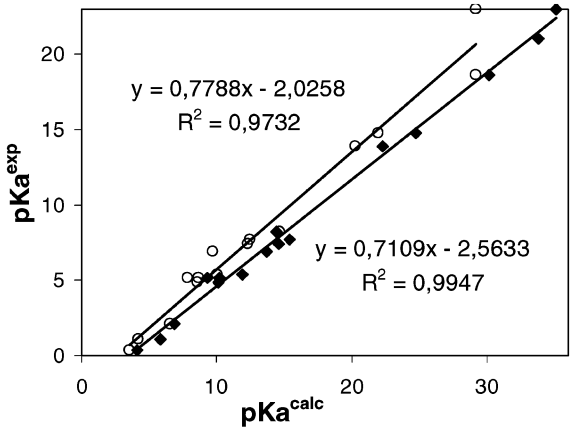

Figure 1. Linear regression of experimental[66] and calculated pK_a values at RHF/6-31G(d) (filled squares), and at RB3LYP/6-311++G(2d,2p) (open circles) levels of theory. Compounds used: 2-methylimidazole, 4-methyilimidazole, benzimidazole, imidazole, quinoline, isoquinoline, piridin, piridazine, pirazine, pirimidine (anion to neutral), 1,2,3,4-tetrazole, 1,2,3-triazole, 1,2,4-triazole, imidazole, pirrole, indole (neutral to cation).

We have demonstrated so far that for rigid nitrogen-containing heterocyclic organic molecules, computed and measured pK_a values correlate significantly. The pK_a value of a specific conformer of flexible molecules was measured only in a few cases, such as for the surface histidine residues of the heme binding protein A.[40] The pK_a of five histidine residues of hemophores (HasA) was measured using NMR spectroscopy.[40] In addition, the conformation of each histidine residue can be derived from the corresponding structure (1b2v[40]). Therefore, we were able to calculate pK_a values by ab initio methods for all five histidine residues with torsion angles assigned in the protein. The comparison of theoretical and experimental pK_a values (Table 1) are as follows. (1) both for His17 ($pK_a^{exp} > 8.1$; $pK_a^{calc} = 9.3$) and His133 ($pK_a^{exp} < 4.6$; $pK_a^{calc} = 3.2$) no precise experimental pK_a values are available but calculated values agree qualitatively with the experimental data. (2) The calculated pK_a values of the other three histidine residues, His83 ($pK_a^{exp} = 5.6$; $pK_a^{calc} = 6.6$), His128 ($pK_a^{exp}=7.1$; $pK_a^{calc}=7.1$), and His32 ($pK_a^{exp}=7.3$; $pK_a^{calc}=7.9$), are in close vicinity of the experimental values. The agreement between experimental and calculated pK_a values is encouraging, especially if we notice that the molecular environment of histidine is completely neglected (i.e., both the neighboring residues and solvation are ignored).

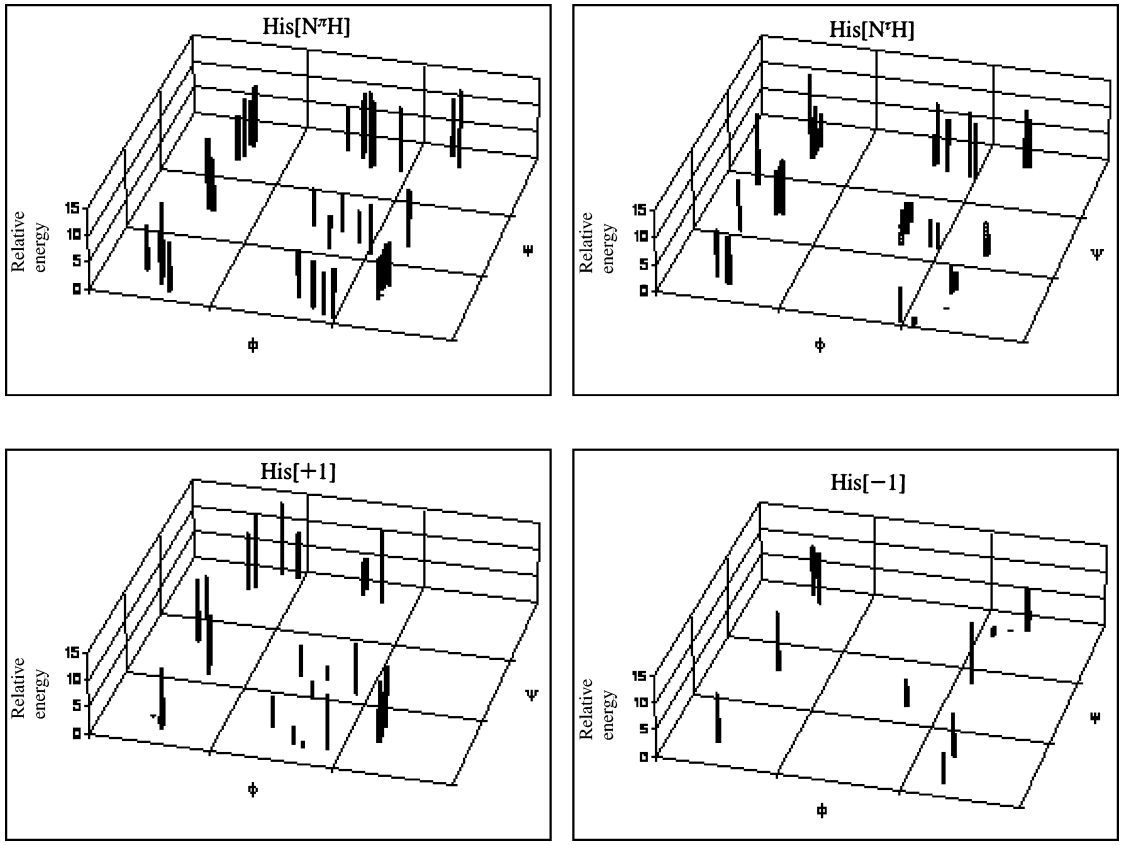

Figure 2. Relative energies (kcal mol^{-1}) of all conformers (129) of *N*-formyl-L-histidinamide as computed at the RHF/6-31G(d) level of theory. Both φ and ψ coordinates are shown from 0° to 360°, catchment regions are given in Figure 3. Characteristic backbone/side chain and side chain/backbone type H-bonds of histidines in proteins: PDB codes, and type of H-bond (Scheme 4) are as follows: 1A2Y and 1AWM stands for type 3 H-bond, while 1ADE for type 4, and 1ALH for type 6.

TABLE 1: pK_a and Selected Geometrical Parameters of Five Histidine Residues in Hemophores (HasA), as Measured by NMR and Calculated at RB3LYP/6-311G++(2d,2p) Level of Theory

residue	φ	ψ	χ_1	χ_2	conf.[a]	pK_a exp[b]	pK_a calc[c]
His17	−59.2	−43.77	171.23	80.2	α_La+	>8.1	9.3
His32	−89.06	81.5	−174.22	97.5	γ_La+	7.3	7.9
His83	57.08	49.23	−58.45	−61.18	α_D− −	5.6	6.6
His128	−72.12	−9.77	−60.99	−178.72	α_L−a	7.1	7.1
His133	−56.2	−53.01	−173.38	−91.62	$\alpha_L$ag−	<4.6	3.2

[a] Backbone and side chain conformation (labeling is explained in methods) of the appropriate His residue in protein. [b] Experimental values are from NMR measurements.[39] [c] Ab initio calculations are for the appropriate conformers of For-L-His-NH_2 (values are scaled according to the linear regression parameters discussed in methods [$m = 0.71$, $b = -2.56$]).

The above examples demonstrate that ab initio calculation of pK_a is a reliable tool in determining molecular properties both for small, rigid molecules and for those of high internal flexibility. Another consideration proved also to be valid, namely that pK_a values of histidine residues in proteins having limited conformational freedom depend primarily on the actual orientation and not on their molecular environment. These results initiated the systematic mapping of PA and pK_a as a function of the molecular conformation now described.

Conformer Stability of *N*-Formyl-L-Histidinamide. A total of 129 different conformers of *N*-formyl-L-histidinamide have been found at the RHF/6-31G(d) level of theory: 43, 43, 28, and 15 for His[N$^{\pi}$H], His[N$^{\tau}$H], His[+1], and His[−1], respectively[3,4] (Figure 2, Tables S1−S4). Under thermodynamic equilibrium in the gas phase, the most populated backbone conformer falls within the γ_L (inverse γ-turn) region for both neutral forms. For the positively charged form α_D (left-handed α-helix) and for the negatively charged form α_L (right-handed α-helix) are the lowest energy backbone conformations (Table 2). The application of a dielectric continuum solvent model (applied dielectric constant was 78.39 as appropriate for water) modifies the thermodynamic equilibrium in favor of the β_L (β-pleated sheet) form. The β_L region of the Ramachandran surface is the most populated one in solution both for the neutral forms as well as for His[−1] (Table 2). (The population distribution of His[+1] remains qualitatively unchanged upon solvation.)

TABLE 2: Relative Population (%) in the Gas Phase and in Solution for Major Backbone (bb) Types of *N*-Formyl-L-histidinamide, Computed at RHF/6-31G(d) Level of Theory[a]

	His[N$^{\pi}$H]		His[N$^{\tau}$H]		His[+1]		His[−1]	
bb type[b]	gas	solvent	gas	solvent	gas	solvent	gas	solvent
γ_L	98	19	57	14	16	29	<1	1
α_L	<1	2	1	13	<1	<1	99	37
β_L	2	76	36	60	2	4	1	61
δ_L	<1	1	7	11	19	16	<1	<1
a_D	<1	2	<1	1	63	51	<1	<1

[a] Populations are calculated from electronic energy values of gas phase and PCM calculations, i.e., $e^{-E_i/RT}/e^{-E_{min}/RT}$, where *i* corresponds to the *i*th conformer. Populations of conformers with their backbone in the same catchment region are summed. [b] Side chain orientations (labeling is explained in methods) are summed for each backbone conformer. (Backbone conformers ϵ_L, ϵ_D and δ_D have negligible relative population in all four forms in both phases, thus not reported.)

The two neutral forms His[N$^{\pi}$H] and His[N$^{\tau}$H] adopt several side chain orientations at each type of backbone fold (Tables S1,S2). The two charged forms, His[+1] and His[−1], have a "complementary" nature, namely structures present for His[−

TABLE 3: Eight Different H-bond Patterns, Assigned in *N*-Formyl-L-histidinamide at the RHF/6-31G(d) Level of Theory (indexation of H-bonds given in Scheme 4)

type of H-bond	torsions involved	orientations of torsions involved	d_1[a]	d_2[a]	ξ[a]
1[b]	φ, ψ	g−, g+ *or* g+, g−	2.18	3.01	140.1
2[c]	φ, ψ	a,a	2.29	2.68	102.3
3[d]	φ, χ_1, χ_2	g+, g+, g− *or* a, g−(a), g+	2.26	3.04	134.8
4[e]	φ, χ_1, χ_2	g−, g−, g+; g−, g+, g−	2.19	2.99	136.3
5[f]	ψ, χ_1, χ_2	a(g+), g+, g+; g−(g+), a, g−	2.10	2.84	129.2
6[g]	ψ, χ_1, χ_2	g−, g+, g+; a, a, g−	2.08	3.01	152.9
7[h]	ψ, χ_1, χ_2	a, g+, g+			
8[i]	φ, χ_1, χ_2	g+, g−, g+	2.49	2.97	109.5

[a] Both the N(O)··H (d_1) and N(O)··N(O) (d_2) distances are in Angstroms, while the N(O)··H−N type bond angles (ξ) are in degrees. Values are taken from selected optimized structures. [b] $NH^{(i+1)}-OC^{(i-1)}$ H-bond forms a seven-member pseudoring of the backbone. The amide proton of the preceding and the carbonyl oxygen of the following amino acid residues are connected. [c] $NH^{(i)}-OC^{(i)}$ H-bond, forms a five-member pseudoring within the backbone. [d] $N^{\pi}H-OC^{(i-1)}$ H-bond, forms an eight-member pseudoring, between backbone and side chain atoms. [e] $NH^{(i)}-N^{\pi}$ H-bond, forms a six-member pseudoring between backbone and side chain atoms. [f] $N^{\pi}H-OC^{(i)}$ H-bond, forms a seven-member pseudoring between backbone and side chain atoms. [g] $NH^{(i+1)}-N^{\pi}$ H-bond, forms a seven-member pseudoring, between backbone and side chain atoms. [h] $N^{\pi}H-N^{(i+1)}$ H-bond, forms a seven-member pseudoring between backbone and side chain atoms. [i] $N^{\pi}H-N^{(i)}$ H-bond, forms a six-member pseudoring between backbone and side chain atoms.

SCHEME 4: Eight Different H-bonds of Histidine Diamide Labeled from 1 to 8 (For typical bond length and bond angle values see Table 3)

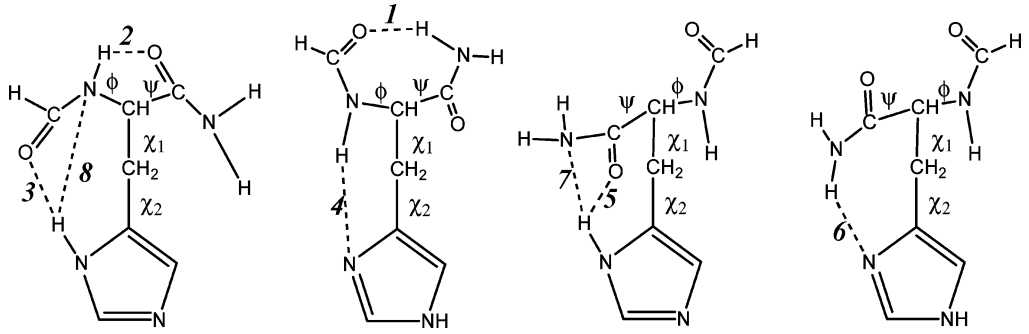

1] are mostly not "available" for His[+1] and vice versa (Tables S3,S4). Monitoring both backbone and side chain orientations, there are only three conformers that are present in all four protonation forms, namely γ_{L}^{-+}, α_{D}^{-+}, and γ_{D}^{--}. As a general conclusion, protonation or deprotonation of histidine typically involves a massive and characteristic conformational change.

Hydrogen Bonds. An important factor that influences and stabilizes the overall fold of histidine in peptides and proteins is the formation of intramolecular hydrogen bonds, which could involve the concerted orientation of selected torsional angles (Table 3). The presence of a particular type of H-bond (1 to 7) in conformers of For-L-His-NH_2 is specified in Tables S1−S4. An H-bond type is typically associated with characteristic torsional angles (Scheme 4). For example, H-bond type 4 locks torsions φ, χ_1 and χ_2, in either g−, g−, g+, or g−, g+, g− orientations, respectively.

The H-bond types of *N*-formyl-L-histidinamide can be classified into two groups. First, there are backbone−backbone type hydrogen bonds (types 1 and 2) that are fully independent of side chain orientation. Both γ_{L}- and γ_{D}-type backbone orientations are stabilized by hydrogen bond type 1: the carbonyl oxygen atom of residue ($i-1$) and the amide proton of residue ($i+1$) form a seven-membered pseudoring. The weak hydrogen bond of β_{L}-type conformers, H-bond type 2, forms a five member pseudoring. These types of H-bonds depend only on the values of the φ and ψ torsional angles. The formation of all four remaining types of hydrogen bonds involve atoms of the imidazole ring, thus depending not only on side chain torsion angles (χ_1 and χ_2) but also either on φ or ψ (Table 3). All backbone−side chain and side chain−backbone type H-bonds were found in proteins (Figure 3).

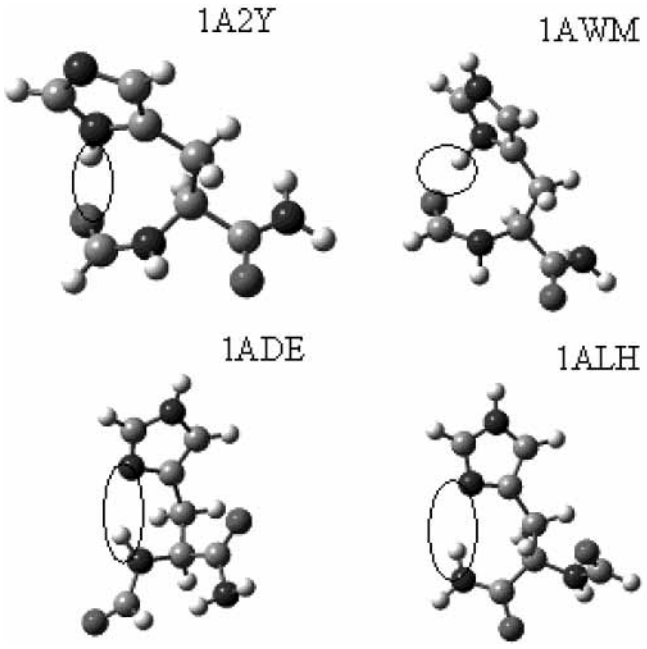

Figure 3. Characteristic backbone/side chain and side chain/backbone type H-bonds of histidines in proteins: PDB codes, and type of H-bond (Scheme 4) are as follows: 1A2Y and 1AWM stands for type 3 H-bond, while 1ADE for type 4, and 1ALH for type 6.

The formation of an intramolecular H-bond is commonly considered to have an energy lowering effect. Thus, the more H-bonds that are present, the lower the expected energy of a conformer.. The average relative energy of the 41 conformers of *N*-formyl-L-histidinamide with no H-bond at all is 9.9 kcal mol^{-1}. For the 75 conformers, where one H-bond is assigned,

the same value decreases to 6.2 kcal mol^{-1}. Moreover, there are 13 different conformers, where two different types of H-bonds were assigned (e.g., α_L++ of His[−1] contains both types 4 and 6 H-bonds). Indeed, the average relative energy above the global minimum of these 13 conformers was computed to be 2.3 kcal mol^{-1}. From these data the average energy lowering effect predicted per H-bond is $\approx 3.8 \pm 0.1$ kcal mol^{-1}.

Establishing an H-bond requires the donation of a proton toward the nonbonding electron pair of a heteroatom. Typically, such interaction cannot be expected from nitrogen atoms of amide systems, since the nonbonding electron pair of this atom is delocalized. However, weak H-bonds can be observed in several histidine conformers between the ring N$^{\pi}$H and the amide N$^{(i+1)}$ atoms. In the case of H-bond type 7 and 8, the planarity of the amide bond is considerably damaged and the nitrogen becomes pyramidal. The existence of these weaker types of hydrogen bonds was also confirmed at higher level calculations: RHF/6-311++G(d,p) and RB3LYP/6-311++G-(d,p). Intramolecular H-bonds have not only a significant stabilizing effect, as discussed so far, but will also influence PA and pK_a.

Proton Affinity. The proton affinity is calculated from the enthalpy change between deprotonated and protonated states (see Methods). As the variation of $\Delta E_v(0)$ and $\Delta E_v(298)$ is within 1 kcal mol^{-1}, the proton affinity differences among conformers is mostly mediated by the electronic energy of the corresponding conformers. The variation of total energy change (and PA) between two forms of protonation is composed of two parts. The first and larger portion corresponds to the acquisition of a proton. The second part is related to the different PEHS of the two forms and to the occasional conformational shift that the molecule undergoes during protonation (or deprotonation). The contribution of the latter effect, i.e., the structural difference between the differently protonated forms, can be neglected if, in average, all torsional angle changes are less than 10°. Proton affinity was calculated for structure pairs (Table 4) where both protonated and deprotonated structures are minima and both belong to the same type of molecular structure. Thus, PAs reported in Table 4 are all associated to a conformer with insignificant structural shift ($\Delta\xi < 10°$, where $\Delta\xi = (\Delta\varphi + \Delta\psi + \Delta\chi_1 + \Delta\chi_2)/4$) upon protonation. Clearly, various conformers may have very different PA values, e.g., PA of His[+1]γ_Lg−g+ → His[N$^{\pi}$H]γ_L−+ is −234.25 kcal mol^{-1}, while that of His[+1]α_D++ → His[N$^{\pi}$H]α_D++ is −245.67 kcal mol^{-1} (Table 4). The averages of these proton affinity values may be considered as the generalized proton affinity of the four protonation pathways of *N*-formyl-L-histidinamide in vacuum. The latter value was calculated to be 238.8 ± 7 kcal mol^{-1} for His[N$^{\pi}$H] → His[+1], 237.6 ± 8 kcal mol^{-1} for His[N$^{\tau}$H] → His[+1], 346.0 ± 4 kcal mol^{-1} for His[−1] → His[N$^{\pi}$H], and 348.1 ± 3 kcal mol^{-1} for the His[−1] → His[N$^{\tau}$H] transition. It is clear that the first protonation step (from negatively charged to neutral) releases ∼120 kcal mol^{-1} more energy than the second one (from neutral to positively charged), so the proton affinity of His[−1] is considerably higher (∼50%) than that of His[N$^{\pi}$H] or His[N$^{\tau}$H].

pK_a. The proton affinity of a molecule or ion in a solvent is characterized by its pK_a value,[67] which requires parameters to be identified for both states of protonation. As the conformers were optimized in both forms of protonation, the orientation of selected torsion angles may be different. This alteration (ξ) is given in Table 4 as an average of the variation of all four major conformational variables, namely, φ, ψ, χ_1, and χ_2. For each

TABLE 4: Proton Affinity (PA in kcal mol^{-1}), pK_a, and Geometry Distorsion Values ($\Delta\xi$ in degrees) of Conformers Existing at Least in Two Protonation Forms for the For-His-NH$_2$ Model Calculated at the RHF/6-31G(d) Level of Theory (conformation labeling is explained in Methods

His[+1] → His[N$^{\pi}$H] + H$^+$

bb.	sc.	PA	pK_a[a]	$\Delta\xi$[b]
γ_L	a−	−239.16	7.46	4.30
	a+	−236.57	7.50	9.77
	−+	−234.25	6.97	4.32
	++	−236.18	7.90	5.08
β_L	−a	−237.23	7.54	5.73
	+−	−238.62	4.65	23.84
	++	−240.13	7.50	7.75
δ_L	a+	−243.31	7.68	3.55
	+g−	−240.20	4.84	24.3
α_D	a−	−242.34	8.00	4.74
	− −	−233.50	6.24	18.90
	−+	−237.68	6.13	26.58
	++	−245.67	9.50	4.91
δ_D	a−	−242.81	7.98	6.78
	a+	−243.01	5.90	25.83
	− −	−236.01	7.86	19.77
ϵ_D	−+	−238.37	6.65	6.14
	+−	−242.16	9.86	17.28
γ_D	aa	−237.54	7.06	8.58
	− −	−232.13	6.78	5.74

His[+1] → His[N$^{\tau}$H] + H$^+$

bb.	sc.	PA	pK_a[a]	$\Delta\xi$[b]
γ_L	a+	−233.71	7.21	8.77
	−+	−229.52	7.11	12.93
β_L	−a	−234.43	7.57	5.86
	+−	−238.15	5.19	17.37
	++	−239.79	8.39	36.74
δ_L	−a	−235.28	7.12	17.93
	+−	−234.87	3.88	46.46
α_D	− −	−230.96	6.20	32.24
	−+	−235.80	6.47	38.80
	+−	−243.82	8.77	29.31
δ_D	a+	−243.61	5.31	23.13
	− −	−237.80	5.98	19.68
ϵ_D	− −	−231.26	6.30	7.28
	++	−237.55	8.81	25.63
γ_D	aa	−235.26	7.03	4.28
	− −	−230.19	6.44	10.05

His[N$^{\pi}$H] → His[−1] + H$^+$

bb.	sc.	PA	pK_a[a]	$\Delta\xi$[b]
γ_L	− −	−347.66	19.94	3.38
	−+	−342.36	20.41	11.31
	+−	−343.79	19.78	21.90
α_L	− −	−346.03	19.26	7.75
β_L	a+	−346.99	17.34	26.78
ϵ_L	+a	−346.86	19.97	24.49
α_D	−+	−345.99	20.69	30.80
ϵ_D	a+	−344.23	18.46	6.18
γ_D	− −	−347.34	21.84	19.65
	−+	−348.19	21.25	31.38

His[N$^{\tau}$H] → His[−1] + H$^+$

bb.	sc.	PA	pK_a*	$\Delta\xi$**
γ_L	− −	−348.72	20.87	5.20
	−+	−347.10	20.27	4.55
	+−	−349.38	20.24	9.58
α_L	− −	−345.99	20.20	10.65
	−+	−345.13	19.20	7.85
β_L	a−	−346.51	18.95	8.18
	a+	−345.82	19.43	3.84
ϵ_L	+a	−349.64	20.15	29.71
α_D	−+	−347.86	20.35	5.61
ϵ_D	a−	−345.51	18.46	2.74
	a+	−346.08	18.60	12.73
γ_D	− −	−349.28	22.18	13.85
	−+	−348.03	21.54	17.87

[a] pK_a values are scaled according to ($m = 0.71$, $b = -2.56$); see Methods for details. [b] $\Delta\xi = (\Delta\varphi + \Delta\psi + \Delta\chi_1 + \Delta\chi_2)/4$.

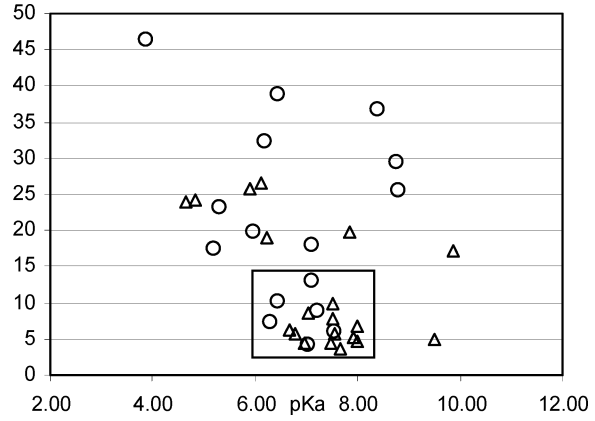

Figure 4. pK_a values of different histidine conformers as function of the conformational shift (difference ($\Delta\xi$) computed for selected torsion angles between protonataed and deprotonated structural counterparts). Structural difference between protonated His[+1] and deprotonated forms (His[N$^{\tau}$H] or His[N$^{\pi}$H]) are computed as follows: $\Delta\xi = (\Delta\varphi + \Delta\psi + \Delta\chi_1 + \Delta\chi_2)/4$. Triangles (△) are for His[+1] → His[N$^{\pi}$H] + H^+ and circles (○) are for His[+1] → His[N$^{\tau}$H] + H^+ deprotonation patterns (Table 4). All pK_a values are within a 2.0 units range (with one exception), if the conformational difference is small ($\Delta\xi < 15°$, area in box).

pair of conformers, pK_a values were computed (Table 4). It should be emphasized, that calculated pK_a values are scaled according to the linear regression parameters ($m = 0.71$, $b = -2.56$) described previously (Figure 1).

For all 16 cases, where the value of $\Delta\xi$ is less than 15°, pK_a values are within a range of 2 units, with a single exception. (Note that both His[+1] → His[N$^{\pi}$H] + H^+ and His[+1] → His[N$^{\tau}$H] + H^+ deprotonation paths are considered.) Interestingly, pK_a values of the His[N$^{\pi}$H] form are on average 0.5 unit higher than those of the His[N$^{\tau}$H] form. For cases, where $\Delta\xi$ is larger, the larger deviation from p$K_a \approx 7$ can also originate from the significant structural difference of the protonated and deprotonated forms (Figure 4).

Conformation-dependent pK_a values associated with the deprotonation of either His[N$^{\tau}$H] or His[N$^{\pi}$H] to His[−1] were also evaluated (Table 4). This type of proton transfer has less biological or chemical significance, which is indicated by the high pK_a values. Nevertheless, in any cases, this pK_a value is also conformation dependent.

Variation of most biologically relevant pK_a values of His is as large as 2.0 units or more, depending on the overall molecular conformation, where conformational shift during protonation is minor or even can be ignored ($\Delta\xi < 15°$). As an example, deprotonation of His[+1] to His[N$^{\pi}$H] occurs at p$K_a = 8.00$ when the backbone is a left-handed helix with an [anti, gauche−] side chain, but the same phenomenon occurs at p$K_a = 6.65$ if the backbone is a mirror image polyproline II structure with a side chain close to gauche−, gauche+ (Table 4). (In both cases $\Delta\xi < 7°$.) This indicates that pK_a of His reflects, in general, the molecular conformation and will be different for different His conformers. Conformation dependent pK_a values associated with the deprotonation of either His[N$^{\tau}$H] or His[N$^{\pi}$H] to His[−1] were also evaluated (Table 4). This type of proton transfer has less biological or chemical significance, which is indicated by the high pK_a values. Nevertheless, in any cases, these pK_a values also show conformation dependence.

Finally, when conformational shift ($\Delta\xi$) during protonation is larger ($25° < \Delta\xi < 45°$), which is rather typical for peptides and proteins, pK_a values of His may vary between 5 and 9, indicating an unexpectedly large conformation dependence.

Discussion

Protonation-Induced Conformational Shifts of Surface Histidine Residues in Proteins. The protonation state of histidine residues on the surface of proteins is influenced by the pH of the solution. Due to the large number of water molecules present, even in the crystal state, the effect of pH can be traced. Histidine residues located at the surface of a macromolecule at lower pH values are protonated (His[+1]), while those at higher pH are neutral (His[N$^{\pi}$H] or His[N$^{\tau}$H]). His[−1] is formed only at such a high pH value that it is an unrealistic condition for folded proteins. During the analysis of X-ray data deposited in PDB, a total of 478 entries were found where the same protein was crystallized at two different pH values: one below pH 5 and one above pH 8. From these pairs of proteins the conformational parameters of histidine residues were retrieved and clustered according to their φ, ψ, χ_1, and χ_2 values. The pairs of histidine residues were classified according to their conformational changes upon proton transfer, which involve only side chains or may also influence backbone torsion angles. A total of 15 examples were collected where the pH induced backbone conformational shift ($\Delta\xi$) is significant, namely, larger than 60° for either φ and/or ψ (Figure 5). In proteins, such a large backbone shift influences the fold of some neighboring residues. Considerably more cases, a total of 287, were found where significant side chain conformational shift (larger than 60° for χ_1 and/or χ_2) of histidine is observed (Figure 5) in protein structures crystallized at the above pH ranges. In the case of histidine residues with the imidazole ring on the surface of the protein, the χ_1 and/or χ_2 conformation is effected upon protonation. The following selected examples of such conformational shifts can be regarded as typical and will be discussed below.

Structural parameters of the complex (biotin-binding protein) streptavidin-cyclo-ac-[CHPQFC]-NH_2 were retrieved from PDB, determined both at pH 11.8 (1vwb[68]) and pH 2.0 (1vwc[68]). His87 in the former structure has an α_D- − orientation, while in the latter one with the same amino acid residue adopts α_D-+ conformation (Table 5). Thus, χ_2 is shifted close to 120° (from g− to g+) due to pH reduction. The latter conformational change upon protonation prevents the formation of a high relative energy conformer of His[+1], the α_D- −. Instead, His[+1] α_D-+ is formed with a relative energy lower by ≈ 5.0 kcal mol^{-1} (Table S3) compared to the α_D- −. The pK_a value of this histidine residue (for proton transfer for His[+1] to His[N$^{\tau}$H]), taking into account the conformational change, is 8.3. However, if the conformation was "frozen" in its high pH state, the pK_a would be equal to 8.0. In contrast to this, if conformation was "frozen" in its low pH form then pK_a would be 11.3. The unexpectedly high pK_a value of the low pH "frozen" conformer approach can be explained with the appearance of an intramolecular H-bond of type 8, stabilizing the protonated state.

There are two available structures of methionine aminopeptidase from hyperthermophile *Pyrococcus furiosus* collected both at pH = 8.5 and pH = 2.6 (1xgm[69] and 1xgo[69]). His161 has a γ_L-+ conformation at higher and a $\gamma_L a+$ at lower pH. The estimated gain in energy (the difference between energy of His[+1] γ_L-+ and His[+1] $\gamma_L a+$) of this conformational shift is ≈2.9 kcal mol^{-1} (Table S3). The pK_a value in this case is near to neutral: 6.9. In addition, pK_a values of low and of high pH conformers using the "frozen" structure approach are similar, 7.1 and 8.0, respectively.

Structures of catalytic domain of human single chain tissue plasminogen activator were also retrieved at two pH values: 8.2 and 4.5 (PDB code: 1a5h[70] and 1bda[71]). His37 adopts β_L-

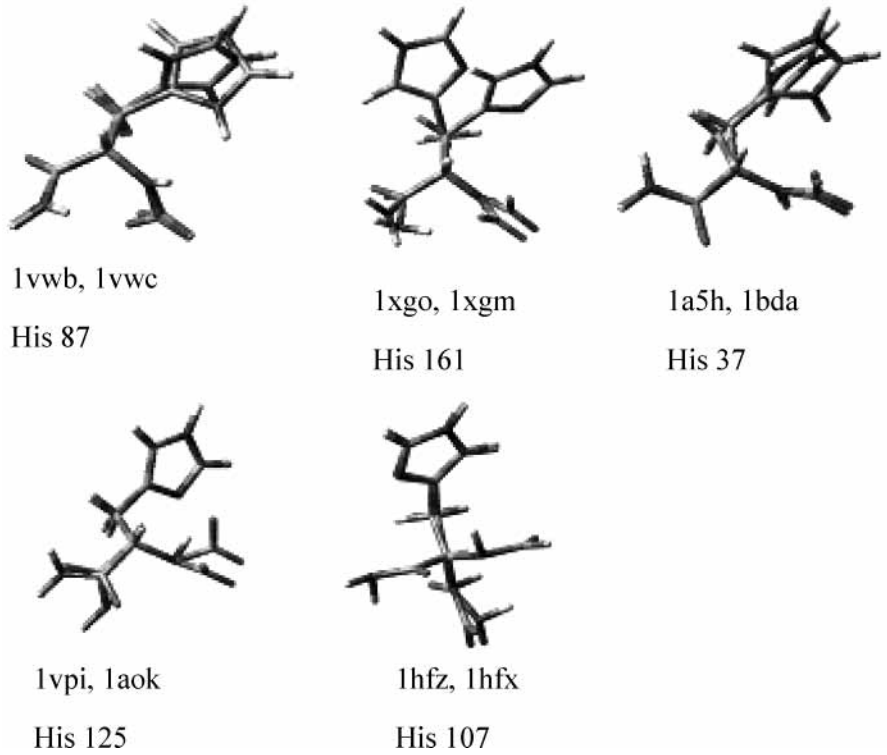

Figure 5. Superimposition of pairs of histidine residues retrieved from protein X-ray structures crystallized at two different pHs: one below 5 and above 8. Selected torsions undergo significant changes, often more than 60°. (See text for details.)

TABLE 5: Conformational Properties of Selected His Residues in Five Different Proteins Crystallized at Two Different pH Values

		high pH state		low pH state				
protein	#His[a]	pH[b]	conf.[c]	pH[b]	conf.[c]	pK_a[d]	pK_a[e]	pK_a[f]
streptavidin derivative	87	11.8	α_D--	2.0	α_D-+	8.3	8.0	11.3
methionine aminopeptidase	161	8.5	γ_L-+	2.6	$\gamma_L a+$	6.9	7.1	8.0
plasminogen activator	37	8.2	β_L-+	4.5	β_L--	5.6	7.9	5.7
vipoxin	125	8.3	α_L-+	4.8	β_L-+	5.4	6.0	6.8
alpha lactalbumin	107	8.0	$\alpha_L a-$	4.3	α_D--	11.0	7.6	10.0

[a] Sequence number of His. [b] pH value, where protein was crystallized. [c] Backbone and side chain conformation (labeling is explained in Methods) of His residue (see text for details). [d] pK_a value taking into account the conformational change between high and low pH states (for neutral state His[N$^\tau$H] form is considered). [e] pK_a value in a "frozen" high pH conformation (for neutral state His[N$^\tau$H] form is considered). [f] pK_a value in a "frozen" low pH conformation (for neutral state His[N$^\tau$H] form is considered).

$+$ conformation at higher pH, and β_L-- at lower pH. The necessity of such conformational change is straightforward since there is no minimum on the PEHS of the His[+1] model system in the region of β_L--. In addition, β_L-+ is not a minimum either for His[N$^\pi$H] or His[N$^\tau$H]. The pK_a values of this histidine conformer with the concerted conformational change is 5.6. The "frozen" structure approach gives values 7.9 and 5.7 in the high and low pH states, respectively (Table 5).

Although their interrelation with pH-induced protonation may involve other effects, two examples are given for backbone conformational shifts. Vipoxin has structures in PDB at pH 8.3 and 4.8 (PDB codes: 1vpi[72] and 1aok[73]). The conformation of His125 is α_L-+ at higher pH and β_L-+ at lower pH. The pK_a value of this histidine residue is 5.4. Low and high pH "frozen" structures have pK_a values of 6.0 and 6.8, respectively. The energy cost of the conformation change from α_L-+ to β_L-+ is estimated to be equal to 3.25 kcal mol^{-1}. Additionally, structure "1aok" is a dimer with numerous van der Waals contacts. The flexible loop of the protein, where His125 is located, is on the surface of the protein monomer. The dimerization influences the conformation of Ile122 and causes some change in the fold of the loop. These two effects, dimerization and protonation-induced conformational shift, are cooperative to get His125 into the more favorable conformational state. As Tyr119 is one of the residues located in the recognition site of the inhibitor, the pH-assisted conformational change may induce the dimerization and play a role in molecular recognition.

Alpha lactalbumin has also been crystallized at high (8.0) and at low (4.3) pH, denoted in PDB as 1hfz[74] and 1hfx,[74] respectively. (The two proteins originate from different species, however, their fold is identical.) His107 is in a flexible loop of the protein having $\alpha_L a-$ conformation at high pH and α_D-- conformation at low pH. Although several flexible loops exist in the protein, the only loop that has significantly different folds at the abovementioned two pH values is the one that contains His107. His107, located on the surface of the protein, at pH = 8 is completely exposed to solvent. Indeed, the same histidine at pH = 4.3 is turned inside of the protein and buried in a hole surrounded by Glu25, Thr29, Ser112, Asn102, and Cys111. At low pH value the buried histidine residue is probably prevented from protontion, since the His[+1]α_D-- structure is a high relative energy conformer. The protection of this histidine from protonation can only be achieved by burying it with other residues because of high a pK_a value (11.0) that would correspond to such a structural change.

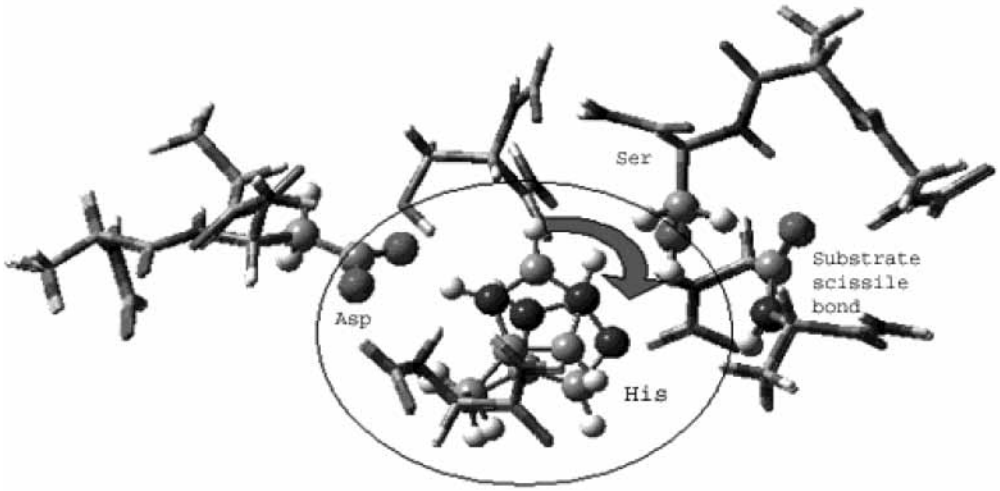

Figure 6. Binding pocket of chymotrypsin (1gl1).[77] Two χ_1 rotamers of His are superimposed: one twisted relative to the other by 20°. This conformational change reduces the distance significantly between the proton to be transferred and the scissile bond. In parallel, the pK_a of histidine is also reduced to "facilitate" proton transfer.

pK_a Change of Buried Histidine during Catalysis. The pK_a value of a histidine residue buried in a protein is determined on one hand by its own conformation, and on the other hand by its molecular environment. Although ab initio calculations on *N*-formyl-L-histidinamide take into account only the conformational properties, nevertheless, in the case of surface residues, the agreement with experimental values is persuading (Table 1). The conformation-dependent changes of pK_a value is of interest not only for His located at the surface of proteins but also for those buried in the core of a protein, such as the case of the His part of the catalytic apparatus of proteases.

The case of proton transfer from one residue to the other within the catalytic triad of serine proteases[75,76] was investigated. Although the catalytic mechanism may involve a number of conformational modifications, a case study is presented to demonstrate that even a small change in geometry might have a number of consequences. As a first step, the catalytic histidine residue acquires a proton from the catalytic serine and transfers it to the nitrogen atom of the scissile amide bond of the substrate. However, the successful proton transfer implies a conformational change of the side chain of the catalytic histidine (Figure 6), namely, a ~20° shift of dihedral angle χ_1. The rotation of χ_1 from the initial 78° (X-ray data) to the optimum value (98°) brings the proton, acquired previously from serine, 0.7 Å closer to the nitrogen of the scissile bond. In addition, the rotation of χ_1 of histidine causes not only a favorable steric proximity of the proton to the scissile bond but it is also energetically preferred. As summarized in Scheme 5 the relative energy difference ($\Delta\Delta E$) is smaller by 2.6 kcal mol^{-1} in the protonated state (ΔE_2 = 1.1 kcal mol^{-1}) than it is in the neutral (ΔE_1 = 3.7 kcal mol^{-1}) form (Scheme 5).

The energy need associated with the side-chain rotation from 78° to 98° is less than one third of that needed when the nitrogen atom of the His side chain's imidazol ring is protonated, compared to the neutral case. Furthermore, the pK_a values associated with χ_1 = 78° and χ_1 = 98° are different, pK_a(I) = 6.6 and pK_a(II) = 5.4, respectively. Therefore, the induced structural change makes the imidazole ring more acidic by 1.2 units (data not scaled).

In short, the unprotonated nitrogen of the catalytic histidine in its neutral form faces toward the catalytic serine. If protonated, a conformational change becomes energetically more advantageous and the imidazole ring turns the acquired proton toward the nitrogen of the scissile bond. Due to this conformational change, the imidazole ring of the catalytic histidine becomes more acidic to facilitate the hydrogen transfer to the nitrogen of the scissile bond.

SCHEME 5: Energy Levels of Protonated and Unprotonated His at Two Suitable χ_1 Side Chain Values Computed at RHF/6-311++G(d,p) Level of Theory

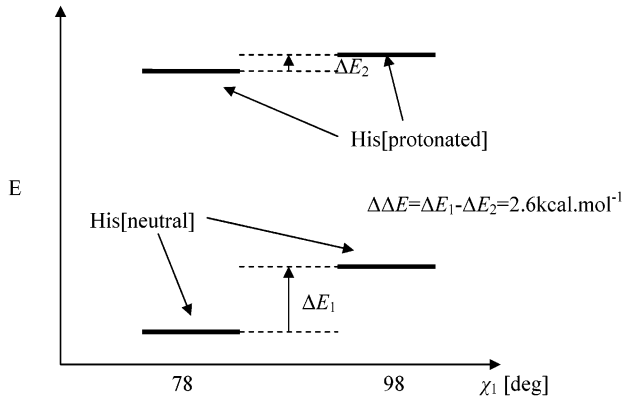

Conclusions

Experimental and calculated pK_a values were compared for small heterocyclic molecules. Their correlation is significant (R^2 = 0.995) supporting the applicability of these theoretical calculations. The agreement of measured and calculated pK_a values of histidine residues in hemophore indicated that pK_a values of various histidine conformers can also be calculated with acceptable precision.

The hydrogen bonds, proton affinity, and pK_a values of the *N*-formyl-L-histidinamide model system were evaluated with respect to all possible conformers. First, the proton affinity and pK_a values were found to be sensitive to the conformation of histidine. Second, we have shown that the protonation (or deprotonation) of the side chain of histidine can induce a considerable amount of conformational change, both for the model system (For-L-His-NH_2) and for histidine residues located in peptides and proteins. Such a conformational change may involve both backbone and/or side chain torsions. Third, for surface histidine the observed conformational changes in X-ray structure determined at different pHs were explained by ab initio results. Fourth, the role of the variation of pK_a was calculated

in the case of the catalytic mechanism of chymotrypsin. The rotation of χ_1 that may accompany the transfer of a proton from serine to the scissile amide bond causes changes in acidity of the histidine side chain. When the nitrogen of the histidine is close to the serine, the imidazole ring has a lower acidity to facilitate the acquisition of the proton from the serine. In the conformation when the proton faces the scissile bond, the elevated acidity ($\Delta pK_a = 1.2$) facilitates the transfer of the proton from histidine to the substrate.

Acknowledgment. The authors thank Imre G. Csizmadia Ödön Farkas, and Ilona Hudáky for helpful discussions. This research was supported by a grant from the Hungarian Scientific Research Foundation (OTKA T047186, TS044730) and by the Wellcome Trust (063822/Z/01/Z). The ELTE computer facility was used for some computations.

Supporting Information Available: Tables S1−S4. Conformational parameters, relative energies, H-bond types, solvation free energies, Gibbs free energies, and enthalpies of For-L-His[N^xH]−NH_2. This material is available free of charge via the internet at http://pubs.acs.org.

References and Notes

(1) Perczel, A.; Ángyán, J. G.; Kajtár, M.; Viviani, W.; Rivail, J.-L.; Marcoccia, J.-F.; Csizmadia I. G. *J. Am. Chem. Soc.* **1991**, *113*, 6256−6265.

(2) Perczel, A.; Hudáky, P.; Csizmadia, I. G. *J. Mol. Struct. (THEOCHEM)* **2000**, *500*, 59−97.

(3) Hudáky, P.; Beke T.; Perczel A. *J. Mol. Struct. (THEOCHEM)* **2002**, *583*, 117−135.

(4) Hudáky, P.; Hudáky, I.; Perczel, A. *J. Mol. Struct. (THEOCHEM)* **2002**, *583*, 199−213.

(5) Noguera, M.; Rodriguez-Santiago, L.; Sodupe, M.; Bertran J. *J. Mol. Struct. (THEOCHEM)* **2001**, *537*, 307−318.

(6) McAllister, M.; A. Perczel, A.; Császár, P.; Viviani, W.; Rivail, J.-L.; Csizmadia I. G. *J. Mol. Struct. (THEOCHEM)* **1993**, *290*, 161−179.

(7) Beachy, M. D.; Chasman, D.; Murphy, R. B.; Halgren, T. A.; Friesner, R. S. *J. Am. Chem. Soc.* **1997**, *119*, 5908−5920.

(8) Schafer, L.; Cao, M.; Ramek, M.; Teppen, B. J.; Newton, S. Q.; Siam, K. *J. Mol. Struct.* **1997**, *413*, 175−204.

(9) Hudáky, P.; Jákli, I.; Császár, A. G.; Perczel, A. *J. Comput. Chem.* **2001**, *22*, 732−751.

(10) Shirazian, S.; Gronert, S. *J. Mol. Struct. (THEOCHEM)* **1997**, *397*, 107−112.

(11) Barroso, M. N.; Cerutti, E. S.; Rodriguez, A. M.; Jauregui, E. A.; Farkas, Ö.; Perczel, A.; Enriz, R. D. *J. Mol. Struct. (THEOCHEM)* **2001**, *548*, 21−37.

(12) Sapse, D. S.; Tong, Y. Z.; Bertino, J. R.; Sapse, A. M. *Cancer Invest.* **1999**, *17*, 396−401.

(13) Perczel, A.; Farkas, Ö.; Csizmadia, I. G. *J. Am. Chem. Soc.* **1996**, *118*, 7809−7817.

(14) Perczel, A.; Farkas, Ö.; Jákli, I.; Csizmadia, I. G. *J. Mol. Struct. (THEOCHEM)* **1998**, *455*, 315−338.

(15) Farkas, Ö.; McAllister, M. A.; Ma, J. H.; Perczel, A.; Hollósi, M.; Csizmadia, I. G. *J. Mol. Struct. (THEOCHEM)* **1996**, *369*, 105−114.

(16) Jákli, I.; Perczel, A.; Farkas, Ö.; Hollósi, M.; Csizmadia, I. G. *J. Mol. Struct. (THEOCHEM)* **1998**, *455*, 303−314.

(17) Hameka, H. F.; Jensen, J. O. *J. Mol. Struct. (THEOCHEM)* **1993**, *107*, 9−16.

(18) Salpietro, S. J.; Perczel, A.; Farkas, Ö.; Enriz R. D.; Csizmadia, I. G. *J. Mol. Struct. (THEOCHEM)* **2000**, *497*, 39−63.

(19) Alemán, C.; Puiggali, J. *J. Phys. Chem. B* **1997**, *101*, 3441−3446.

(20) Tarditi, A. M.; Klipfel, M. W.; Rodriguez, A. M.; Suvire, F. D.; Chasse, G. A.; Farkas, Ö.; Perczel, A.; Enriz, R. D. *J. Mol. Struct. (THEOCHEM)* **2001**, *545*, 29−47.

(21) Masman, M. F.; Amaya, M. G.; Rodriguez, A. M.; Suvire, F. D.; Chasse, G. A.; Farkas, Ö.; Perczel, A.; Enriz, R. D. *J. Mol. Struct. (THEOCHEM)* **2001**, *543*, 203−222.

(22) Baldoni, H. A.; Rodriguez, A. M.; Zamora, M. A.; Zamarbide, G. N.; Enriz, R. D.; Farkas, Ö.; Császár, P.; Torday, L. L.; Sosa, C. P.; Jákli, I.; Perczel, A.; Papp, J. Gy.; Hollósi, M.; Csizmadia, I. G. *J. Mol. Struct. (THEOCHEM)* **1999**, *465*, 79−91.

(23) Ramek, M.; Kelterer, A.-M.; Nikolic, S. *Int. J. Quantum Chem.* **1997**, *65*, 1033−1045.

(24) Kang, Y. K. *J. Phys. Chem.* **1996**, *100*, 11589−11595.

(25) Fischer, S.; Dunbrack, R. L.; Karplus M. *J. Am. Chem. Soc.* **1994**, *116*, 11931−11937.

(26) Zamora, M. A.; Baldoni, H. A.; Bombasaro, J. A.; Mak, M. L.; Perczel, A.; Farkas, Ö.; Enriz R. D. *J. Mol. Struct. (THEOCHEM)* **2001**, *540*, 271−283.

(27) Fernandez-Ramos, A.; Cabaleiro-Lago, E.; Hermida-Ramon, J. M.; Martinez-Nunez, E.; Pena-Gallego A. *J. Mol. Struct. (THEOCHEM)* **2000**, *498*, 191−200.

(28) IUPAC Commission on the Nomenclature of Organic Chemistry CNOC and IUPAC−IUB Commission on Biochemical Nomenclature CBN, Nomenclature of −Amino Acids, Recommendations 1974, (a) *Biochem. J.* **1975**, *149*, 1−16 (b) *Biochemistry* **1970**, *9*, 3471−3479.

(29) Cheng, F.; Zhang, R.; Zhang, X.; Shen, J.; Li, X.; Gu, J.; Zhu, W.; Shen, J.; Sagi, I.; Ji, R.; Chen, K.; Jiang H. *J. Phys. Chem. B.* **2002**, *106*(17), 4552−4559.

(30) Hasegawa, K.; Ono, T.; Noguchi T. *J. Phys. Chem. B* **2000**, *104*, 4253−4265.

(31) Bliznyuk, A. A.; Schaefer, H. F.; Amster I. J. *J. Am. Chem. Soc.* **1993**, *115*, 5149−5154.

(32) No, K. T.; Cho, K. H.; Kwon, O. Y.; Jhon, M. S.; Scheraga H. A. *J. Phys. Chem.* **1994**, *98*, 10742−10749.

(33) Ash, E. L.; Sudmeier, J. L.; Day, R. M.; Vincent, M.; Torchilin, E. V.; Haddad, K. C.; Bradshaw, E. M.; Sanford, D. G.; Bachovchin W. W. *P. Natl. Acad. Sci. U.S.A.* **2000**, *97(19)*, 10371−10376.

(34) Nishihira, J.; Tachikawa, H. *J. Theor. Biol.* **1999**, *196*, 513−519.

(35) Müller, J. D.; McMahon, B. H.; Chien, E. Y. T.; Sligar, S. G.; Nienhaus G. U. *Biophys. J.* **1999**, 1036−1051.

(36) Mangs, H.; Sui, G. C.; Wiman B. *FEBS Lett.* **2000**, *475*, 192−196.

(37) Tjalsma, H.; Stover, A. G.; Driks, A.; Venema, G.; Bron, S.; Dijl J. M. *J. Biol. Chem.* **2000**, *275*, 25102−25108.

(38) Gubba, S.; Cipriano, V.; Musser, J. M. *Infect. Immun.* **2000**, *68*, 3716−3719.

(39) Tseng, C. C.; Miyamoto, M.; Ramalingam, K.; Hemavathy, K. C.; Levine, M. J.; Ramasubbu, N. *Arch. Oral. Biol.* **1999**, *44*, 119−127.

(40) Wolff, N.; Deniau, C.; Létoffé, S.; Simenel, C.; Kumar, V.; Stojiljkovic, I.; Wandersman, C.; Delepierre, M.; Lecroisey, A. *Protein Sci.* **2002**, *11*, 757−765.

(41) Villa, J.; Warshel A. *J. Phys. Chem. B* **2001**, *105*(33), 7887−7907.

(42) Kubicki, M.; Borowiak, T.; Dutkiewicz, G.; Souhassou, M.; Jelsch, C.; Lecomte C. *J. Phys. Chem. B.* **2002**, *106*(14), 3706−3714.

(43) Dölker, N.; Maseras, F.; Lledós, A. *J. Phys. Chem. B* **2001**, *105*(31), 7564−7571.

(44) Blomberg, M. R. A.; Siegbahn, P. E. M. *J. Phys. Chem. B* **2001**, *105*(39), 9375−9386.

(45) Torrent, M.; Mogi, K.; Basch, H.; Musaev, D. G.; Morokuma K. *J. Phys. Chem. B.* **2001**, *105*(36), 8616−8628.

(46) Walker, R. C.; de Souza, M. M.; Mercer, I. P.; Gould, I. R.; Klug, D. R. *J. Phys. Chem. B* **2002**, *106*(44), 11658−11665.

(47) Frisch, M. J.; Trucks, G. W.; Schlegel, H. B.; Scuseria, G. E.; Robb, M. A.; Cheeseman, J. R.; Zakrzewski, V. G.; Montgomery, J. A.; Stratmann, R. E.; Burant, J. C.; Dapprich, S.; Millam, J. M.; Daniels, A. D.; Kudin, K. N.; Strain, M. C.; Farkas, O.; Tomasi, J.; Barone, V.; Cossi, M.; Cammi, R.; Mennucci, B.; Pomelli, C.; Adamo, C.; Clifford, S.; Ochterski, J.; Petersson, G. A.; Ayala, P. Y.; Cui, Q.; Morokuma, K.; Salvador, P.; Dannenberg, J. J.; Malick, D. K.; Rabuck, A. D.; Raghavachari, K.; Foresman, J. B.; Cioslowski, J.; Ortiz, J. V.; Baboul, A. G.; Stefanov, B. B.; Liu, G.; Liashenko, A.; Piskorz, P.; Komaromi, I.; Gomperts, R.; Martin, R. L.; Fox, D. J.; Keith, T.; Al-Laham, M. A.; Peng, C. Y.; Nanayakkara, A.; Challacombe, M.; Gill, P. M. W.; Johnson, B.; Chen, W.; Wong, M. W.; Andres, J. L.; Gonzalez, C.; Head-Gordon, M.; Replogle, E. S.; Pople, J. A. Gaussian 98 Revision A.11.1; Gaussian, Inc.: Pittsburgh, PA, 2001.

(48) Roothaan C. C. J. *Rev. Mod. Phys.* **1951**, *23*, 69−89.

(49) Hehre, W. J.; Radom, L.; Schleyer, P. v. R.; Pople, J. A. Ab Initio Molecular Orbital Theory; Wiley-Interscience: New York, 1986.

(50) Ditchfield, R.; Hehre, W. J.; Pople, J. A. *J. Chem. Phys.* **1971**, *54*, 724.

(51) Hehre, W. J.; Ditchfield, R.; Pople, J. A. *J. Chem. Phys.* **1972**, *56*, 2257.

(52) Gordon, M. S. *Chem. Phys. Lett.* **1980**, *76*, 163−168.

(53) Delbene, J. E.; Mettee, H. D.; Frisch, M. J.; Luke, B. J.; Pople, J. A. *J. Phys. Chem.* **1983**, *87*, 3279−3282.

(54) Castro, G. T.; Giordano, O. S.; Blanco, S. E. *J. Mol. Struct. (THEOCHEM)* **2003**, *626*, 167−178.

(55) Fogolari, F.; Brigo, A.; Molinari, H. *J. Mol. Recognit.* **2002**, *15*, 377−392.

(56) Guthrie, J. P.; O'Ferral, R. A. M.; O'Donoghue, A C.; Waghorne, W. E.; Zrinski, I. *J. Phys. Org. Chem.* **2003**, *16*, 582−587.

(57) Namazian, M.; Heidary, H. *J. Mol. Struct. (THEOCHEM)* **2003**, *620*, 257−263.

(58) Nielsen, J. E.; McCammon, J. A. *Protein Sci.* **2003**, *12*, 1894−1901.

(59) Pliego, J. R. *Chem. Phys. Lett.* **2003**, *367*, 145−149.

(60) Reniero, F.; Guillou, C.; Frassineti, C.; Ghelli, S. *Anal. Biochem.* **2003**, *319*, 179−194.
(61) Lim, C.; Bashford, D.; Karplus, M. *J. Phys. Chem.* **1991**, *95*, 5610−5620.
(62) Miertus, S.; Scrocco, E.; Tomasi, J. *Chem. Phys.* **1981**, *55*, 117−129.
(63) Mejias, J. A.; Lago S. *J. Chem. Phys* **2000**, *113*, 7306−7316.
(64) Bernstein, F. C.; Koetzle, T. F.; Williams, G. J.; Meyer, E. E.; Brice, M. D.; Rodgers, J. R.; Kennard, O.; Shimanouchi, T.; Tasumi M. *J. Mol. Biol.* **1977**, *112*, 535−542.
(65) Ramakrishnan, C.; Ramachandran, G. N. *Biophys. J.* **1965**, *5*, 909.
(66) Bruice, T. C.; Schmir, G. L. *J. Am. Chem. Soc.* **1958**, *80*, 148.
(67) Grycuk, T. *J. Phys. Chem. B* **2002**, *106*(6), 1434−1445.
(68) Katz, B. A.; Cass, R. T. *J. Biol. Chem.* **1997**, *272*, 13220−13228.
(69) Tahirov, T. H.; Oki, H.; Tsukihara, T.; Ogasahara, K.; Yutani, K.; Ogata, K.; Izu, Y.; Tsunasawa, S.; Kato, I. *J. Mol. Biol.* **1998**, *284*, 101−124.
(70) Renatus, M.; Engh, R. A.; Stubbs, M. T.; Huber, R.; Fischer, S.; Kohnert, U.; Bode, W. *Embo J.* **1997**, *6*, 4797−4805.
(71) Renatus, M.; Bode, W.; Huber, R.; Sturzebecher, J.; Prasa, D.; Fischer, S.; Kohnert, U.; Stubbs, M. T. *J. Biol. Chem.* **1997**, *272*, 21713−21719.
(72) Devedjiev, V.; Popov, A.; Atanasov, B.; Bartunik H. D. *J. Mol. Biol.* **1997**, *266*, 160−172.
(73) Perbandt, M.; Wilson, J. C.; Eschenburg, S.; Mancheva, I.; Aleksiev, B.; Genov, N.; Willingmann, P.; Weber, W.; Singh, T. P.; Betzel, C. *FEBS Lett.* **1997**, *412*, 573−577.
(74) Pike, A. C.; Brew, K.; Acharya, K. R. *Structure London* **1996**, *4*, 691−703.
(75) Venekei, I.; Szilágyi, L.; Gráf, L.; Rutter, W. J. *FEBS Lett.* **1996**, *379*, 143−147.
(76) Gráf, L. *Natural Sciences and Human Thought*; Zwilling, Ed.; Springer-Verlag: Berlin, Heidelberg, 1995; pp 139−148.
(77) Roussel, A.; Mathieu, M.; Dobbs, A.; Luu, A.; Cambillau, C.; Kellenberger, C. *J. Biol. Chem.* **2001**, *276*, 38893−38898.